CrossMark

J. Fluid Mech. (2017), *vol.* 812, *pp.* 349–369. © Cambridge University Press 2016
doi:10.1017/jfm.2016.802

Segregation in dissolving binary-component sessile droplets

Erik Dietrich[1,2], Maaike Rump[1,2], Pengyu Lv[1], E. Stefan Kooij[2], Harold J. W. Zandvliet[2,†] and Detlef Lohse[1,3,†]

[1]Physics of Fluids, MESA+ Institute for Nanotechnology and J. M. Burgers Centre for Fluid Dynamics, University of Twente, P.O. Box 217, 7500 AE Enschede, The Netherlands

[2]Physics of Interfaces and Nanomaterials, MESA+ Institute for Nanotechnology, University of Twente, P.O. Box 217, 7500 AE Enschede, The Netherlands

[3]Max Planck Institute for Dynamics and Self-Organization, 37077 Goettingen, Germany

(Received 20 May 2016; revised 21 November 2016; accepted 23 November 2016; first published online 28 December 2016)

The dissolution of a single droplet, containing a mixture of oils, in water is experimentally studied. The oils in the droplet varied in terms of their solubility in water and their hydrophobicity. We demonstrate that the polarity of the droplet constituents strongly influences the dissolution dynamics. A binary-component droplet, containing two polar components (one soluble the other insoluble) exhibits a retarded dissolution as compared to a droplet containing only the soluble component. We argue that in this case the mixture in the droplet can be assumed homogeneous, leading to a smaller effective contact area of the soluble liquid in the droplet with the bulk water, and thus delayed dissolution. On the other hand, it is shown that this is not the case when a polar, soluble component is mixed with an insoluble non-polar component, in which case segregation between the different liquids inside the droplet occurs, leading to Marangoni flows and superspreading of the droplet. The segregation is confirmed by volumetric measurements and by the use of a solvatochromic dye in combination with confocal microscopy, which clearly showed that during dissolution local concentration differences inside the droplet developed.

Key words: convection, drops and bubbles, plumes/thermals

1. Introduction

The evaporation of a liquid droplet in air and the dissolution of gas bubbles or liquid droplets in water are comparable processes that have received much attention in the past decades (Cazabat & Guena 2010; Erbil 2012; Lohse & Zhang 2015). The topic of droplet evaporation and dissolution owes its popularity to its relevance in many applications. The first analytical description was given by Epstein & Plesset (1950) in the context of diffusive transport from a spherical gas bubble in water, and has since then been extended to describe evaporating and dissolving sessile droplets (Picknett & Bexon 1977; Popov 2005; Lohse & Zhang 2015; Zhang *et al.* 2015). Especially the evaporation of sessile droplets has been studied in detail, revealing the

†Email addresses for correspondence: h.j.w.zandvliet@utwente.nl, d.lohse@utwente.nl

https://doi.org/10.1017/jfm.2016.802 Published online by Cambridge University Press

influence of e.g. the effect of the thermal conductivity of the substrate (Dunn *et al.* 2009; Sobac & Brutin 2012), substrate wettability (Talbot *et al.* 2012), the behaviour of the contact angle during evaporation (Bourges-Monnier & Shanahan 1995; Guéna, Poulard & Cazabat 2006) and the influence thereof on the evaporation time (Stauber *et al.* 2014; Stauber, Wilson & Duffy 2015*a*; Stauber *et al.* 2015*b*), pinning of the contact line (Shanahan 1995; Moffat, Sefiane & Shanahan 2009; Dietrich *et al.* 2015), natural convection around the droplet (Kelly-Zion, Batra & Pursell 2013; Somasundaram, Anand & Bakshi 2015; Dietrich *et al.* 2016), cooling of the droplet surface (Dehaeck, Rednikov & Colinet 2014), particles inside the droplet (Nguyen & Nguyen 2012) and the effect of the droplet liquid on the evaporation process (Kelly-Zion *et al.* 2009). Despite the large number of publications on the topic, most of the experimental and theoretical efforts by the (sessile) droplet community have been directed towards droplets containing only a single component.

The focus on single-component sessile droplets is contrasted by a considerable body of research conducted on the vaporization and evaporation of multi-component (automotive) fuel sprays, which has been a topic of research for decades (Aggarwal & Peng 1995; Tan *et al.* 2016). While this topic is dominated by different physical processes (for example a strong emphasis on non-isothermal processes and forced convection (Abramzon & Sirignano 1989)), similar approaches to the multi-component problem have been utilized as in the topic of the current work: dissolution of binary-component sessile droplets in clean water. An example of a dissolving binary-component sessile droplet is shown in figure 1. Panels (*a–c*) show photographs of a droplet which contains a mixture of pentanol and cyclohexane, immersed in clean water in which it slowly dissolves.

When a droplet of a certain material a is placed in an immiscible, stationary bulk, an interface will form as shown in figure 1(*a*). If material a is soluble in the bulk and the bulk is clean (i.e. it does not contain any dissolved materials), molecules of a at the droplet side of the interface will cross the interface and dissolve into the bulk, saturating the bulk close to the interface of the droplet to $c_{s,a}$, the saturation concentration of material a in the bulk. Far away from the droplet, the bulk is assumed to be clean ($c_{\infty,a} = 0$), which sets up a concentration gradient that drives the dissolved material away from the droplet at a rate characterized by the diffusion coefficient D_a of a through the bulk. This 'makes room' at the droplet interface for more of the droplet material to dissolve, ultimately leading to complete dissolution of the droplet. When the droplet contains a second component b, miscible with a but immiscible with the bulk, the effective droplet dissolution rate will be altered, depending on the properties and concentrations of a and b. Such a mixture can be described in multiple ways, for example by considering the mixture as a single, continuous liquid, the properties of which depend on the constituents (Kneer *et al.* 1993; Tamim & Hallett 1995; Burger *et al.* 2003). Because this method does not explicitly consider the individual components and concentrations in the description of the dissolution or evaporation process, it makes this method a suitable approach to describe droplets which contain many components (Sazhin *et al.* 2010). Other methods do treat the droplet components on an individual basis, and consider the contribution of each of the components with its respective properties. This is best illustrated by Brenn *et al.* (2007), who explicitly considered the total evaporation rate of their (spherical) fuel droplets as the sum of the rates at which the individual components $i = a, b$ evaporate:

$$\frac{\mathrm{d}m}{\mathrm{d}t} = \sum_{i=a,b} \frac{\mathrm{d}m_i}{\mathrm{d}t}. \tag{1.1}$$

https://doi.org/10.1017/jfm.2016.802 Published online by Cambridge University Press

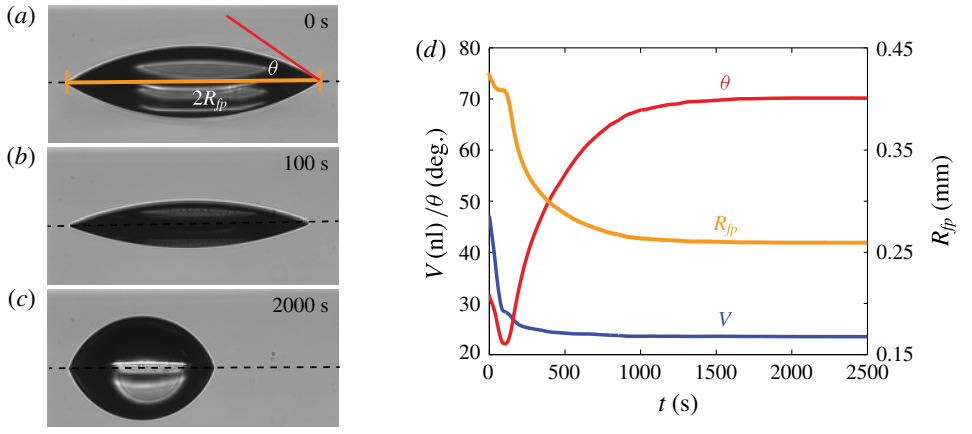


FIGURE 1. (Colour online) Panel (*a*) side view photograph of a sessile droplet, placed on a water-immersed hydrophobic substrate (indicated by the dashed line). A mirror image of the droplet is produced by the reflective substrate. The droplet, which has an initial volume $V_0 = 46$ nl contains pentanol mixed with cyclohexane in a 1:1 ratio (measured by volume). During the first ≈200 s, the soluble pentanol rapidly dissolves and the droplet volume V decreases while the footprint radius R_{fp} initially decreases slightly, after which it remains constant, leading to a decreasing contact angle θ, as illustrated by the photograph in panel (*b*), and the graph in panel (*d*). As the volume of the droplet decreased to ≈25 nl, the dissolution quickly slows down until only the insoluble cyclohexane remains and V remains constant at $V = 23$ nl. In this final stage, θ slowly increases again, causing the droplet footprint to contract, as illustrated in panel (*c*) and the graph in panel (*d*). The irregularity visible in V around $t = 100$ s is due to movement out of the focal plane, causing a slight shift in the perceived size of the droplet. The dashed lines in panels (*a–c*) mark the droplet contact line.

Instead of using the droplet diameter R in calculating $\mathrm{d}m_i/\mathrm{d}t$, Brenn *et al.* (2007) introduced the volume equivalent partial radius $R_{V,i} = R\phi_i^{1/3}$, using the instantaneous volume fraction ϕ_i of each of the components. To calculate $\mathrm{d}m_i/\mathrm{d}t$, the material properties ($c_{s,i}$, D_i and liquid density ρ_i) must be known, as well as the concentrations of the materials on both sides of the droplet–bulk interface. In droplet vaporization, Raoult's law ($P_i = x_i P_i^*$, with P_i the partial vapour pressure of component i in the bulk, x_i the mole fraction of i in the liquid and P_i^* the vapour pressure of the pure component) is commonly used for this purpose (Lehmann *et al.* 2015; Tonini & Cossali 2016). However, this is an approximation, as Raoult's law relies on an ideal gas and thus neglects any interaction between the materials, and various methods have been presented to account for this (Sazhin *et al.* 2010; Zhang & Kong 2012; Tonini & Cossali 2015).

In 2013, Su & Needham (2013) presented one of the first studies on multi-component droplet dissolution in water. They assumed the instantaneous droplet–bulk interface composition of their spherical droplets, containing a mixture of two different types of acetates, to be directly related to the droplet volumetric composition:

$$\frac{V_a}{V_b} = \frac{A_a}{A_b}, \tag{1.2}$$

where V_i and A_i are the volume and area fractions of the droplet–bulk interface respectively, occupied by components $i = a, b$ (denoted by the subscripts) such that

https://doi.org/10.1017/jfm.2016.802 Published online by Cambridge University Press

the total droplet volume $V = V_a + V_b$, and interfacial area $A = A_a + A_b$. Instead of a volume equivalent partial droplet radius, Su and Needham calculated the dissolution rate of the individual components based on the total droplet radius, and multiplied this by the surface area fraction $A_i/A \leqslant 1$ occupied by the respective component, equivalent to the approach by Brenn *et al.* (2007). Note that while (1.2) describes the composition at the droplet side of the droplet/bulk interface, it is equivalent to the use of Raoult's law to determine the partial gas pressures at the bulk side of the interface, in the sense that both approaches assume negligible interaction between a and b and a homogeneous mixture inside the droplet.

Although Su and Needham obtained good agreement between their theoretical model and experiments, the assumption of perfect mixing and the absence of an interaction between a, b and possibly the bulk, has been questioned. In fact, Su and Needham already noted that their approach could not be used in core–shell systems.

To overcome this limitation, the interaction between a, b and the bulk has to be incorporated. A so-called activity coefficient γ_i for each component can be introduced to describe this interaction, and has been used to either correct Raoult's law (Brenn *et al.* 2007; Sazhin *et al.* 2010), or as shown very recently by Chu & Prosperetti (2016), the surface area distribution. The activity coefficient expresses the interaction between the different species, based on their concentrations and the molecular structures.

In this paper we study the dissolution of oil droplets in clean water to experimentally test the applicability of the approaches put forward by Su & Needham (2013) and Chu & Prosperetti (2016). To this purpose, the droplets contain binary mixtures of water soluble long-chain primary alcohols (pentanol or heptanol), and compounds which are fully miscible with the alcohol but insoluble in water (cyclohexane or decanol). By using these combinations we combine a polar, soluble compound with a water-insoluble material that is either also polar (decanol), or non-polar (cyclohexane). We compare the dissolution of these mixtures to existing theory, and to the dissolution dynamics of fully soluble single-component droplets.

2. Experimental procedure

2.1. *Preparation and materials*

Figure 2(*a*) provides a sketch of the experimental set-up. The substrates were $\approx 1 \times 1$ cm^2 pieces of a single side polished silicon wafer (P-type, boron doped (100) oriented, Okmetic) coated with PFODMS (1H, 1H, 2H, 2H-Perfluoroctyldimethylchlorosilane 97 %, ABCR GmbH, Karlsruhe Germany) following the procedure described earlier (Dietrich *et al.* 2015). The PFODMS molecules bind covalently to the silicon substrate, forming a densely packed hydrophobic monolayer. After the coating procedure, the samples were cleaned by insonication in chloroform for 10 min to remove any unbound silanes and dried under a stream of nitrogen gas. Prior to each experiment, the samples were cleaned by insonication in acetone and dried under a stream of nitrogen. The sample was positioned at the bottom of a cubical glass tank with dimensions $5 \times 5 \times 5$ cm^3. Subsequently, the tank was filled with 100 ml water obtained several hours before the experiment (to allow for thermal equilibration) from a purifier (Reference A+, Merck Millipore, at 18.2 MΩcm). Finally, a droplet was placed on the immersed sample from a glass syringe through a thin (210 μm outer diameter) needle. The syringe was vertically mounted in a computer controlled motorized pump, allowing to dispense droplets of controlled volumes.

https://doi.org/10.1017/jfm.2016.802 Published online by Cambridge University Press

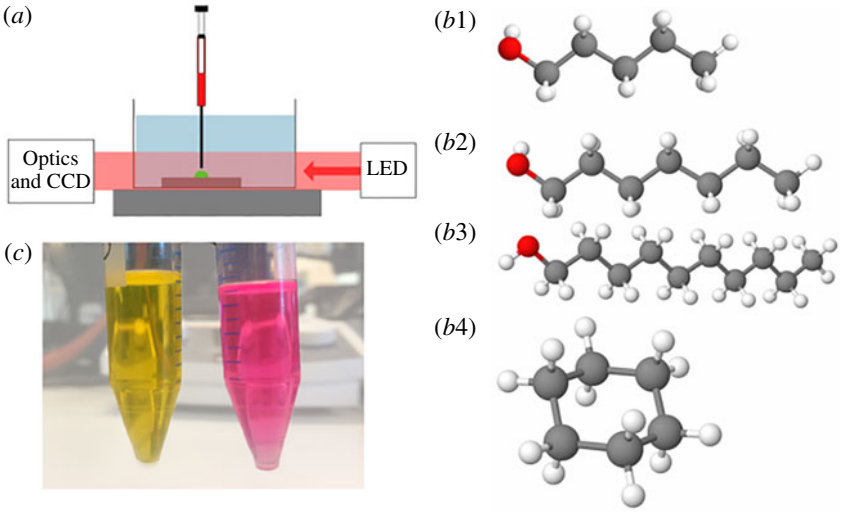


FIGURE 2. (Colour online) (*a*) Sketch of the experimental set-up (not to scale) showing the droplet (in green) on the substrate in the glass tank. The syringe is mounted in a computer controlled pump (not drawn) to dispense the droplets. An LED source illuminates the droplet, and projects the image through a long-distance microscope onto a charge coupled device camera. Panel (*b*) shows the molecular structures of the primary alcohols pentanol (*b*1), heptanol (*b*2), decanol (*b*3) and cyclohexane (*b*4). Grey, red and white spheres represent carbon, oxygen and hydrogen atoms, respectively. (*c*) Shows how the emission wavelength of Nile red dye depends on the polarity of the solvent. It appears yellow in a non-polar solvent such as cyclohexane (left tube), but purple when a polar compound is added, as visible in the pentanol/cyclohexane mixture (right tube).

All liquids were obtained from Sigma-Aldrich at $\geqslant 98\,\%$ purity, and used without further purification. The relevant properties of the materials are listed in table 1, together with the advancing and receding contact angles (θ_A and θ_R, respectively) as measured in multiple inflate–deflate cycles of a sessile droplet on water-immersed PFODMS-coated silicon substrates. Binary mixtures of the liquids were prepared by premixing the two liquids at the desired volumetric ratios in clean glass-stoppered flasks, from which the syringe was filled. As cyclohexane is very volatile, the 100 µl syringe was refilled with a fresh mixture at the beginning of each experiment, subsequently flushed with ≈ 10 µl, after which the droplet was quickly deposited. However, small variations in initial droplet composition could not be ruled out, mainly due to variations in the set-up time of the experiment: a short amount of time between droplet deposition and the start of the recording was required to focus the microscope on the droplet. During this set-up time, the droplet had already started to dissolve to a certain degree. This set-up time however was small (less than a minute), compared to the total duration of the experiment, so that the difference was limited, as can be seen later on.

2.2. *Imaging*

The droplet was illuminated by a collimated light emitting diode (LED) light source (Thorlabs, wavelength $\lambda = 625$ nm) and imaged by a charge coupled device camera (Pixelfly USB, PCO Germany), fitted with a long-distance microscope with

https://doi.org/10.1017/jfm.2016.802 Published online by Cambridge University Press

Material	ρ (kg m^{-3})	D (10^{-9} m^{2}s^{-1})	c_s (kg m^{-3})	$\Delta\rho$ (kg m^{-3})	γ mN m^{-1}	Dipole moment (Debye)	θ_A (deg.)	θ_R (deg.)
Pentanol	811	0.888[e]	22[a,b]	3.42	4.4[d]	1.7[i]	50 ± 7	43 ± 6
Heptanol	822	0.800[e]	1.67[b]	0.29	7.7[d]	1.739[j]	60 ± 1	50 ± 2
Decanol	830	0.475[f]	0.036[f]	≈ 0	8.97[g]	1.6[h]	68 ± 1	53 ± 1
Cyclohexane	778	0.839[k]	0.043[c]	≈ 0	50[d]	0[i]	89 ± 6	69 ± 8

TABLE 1. Properties of the various materials used in this work (measured at 25 °C): chemical composition, density ρ of the pure liquid, diffusion constant D of the material in water, saturation solubility c_s in water, interfacial tension γ of the liquid–water interface, dipole moment of the molecule and the advancing (θ_A) and receding contact angles (θ_R) for a sessile droplet of the material on a PFODMS-coated Si substrate, immersed in clean water. The density difference $\Delta\rho = \rho_{H_2O} - \rho_{sat}$ between clean water and water saturated with the respective alcohol was calculated using the data from Høiland & Vikingstad (1976). No values for $\Delta\rho$ of decanol and cyclohexane could be found, and given their negligible solubility it is safe to assume $\Delta\rho \approx 0$.

[a]Other data were obtained from Crittenden & Hixson (1954).
[b]Kinoshita, Ishikawa & Shinoda (1958).
[c]Hansch, Quinlan & Lawrence (1968).
[d]Demond & Lindner (1993).
[e]Hao & Leaist (1996).
[f]Addison & Hutchinson (1949).
[g]Hastings *et al.* (2013).
[h]Stenutz (2015).
[i]Haynes (2004).
[j]Yaws (2014).
[k]GSI Environmental (2016).

adjustable magnification. The images were obtained at a typical rate of 1 f.p.s., and post-processed using a Matlab routine to extract the droplet profile with sub-pixel accuracy (van der Bos *et al.* 2014). The microscope was focussed on the droplet at the beginning of the experiment. The needle (with a measured outer diameter of 210 μm) was used to calibrate the image. This method was validated by measuring (hemi)spherical solid objects of known dimensions, leading to good agreement. Pinning or depinning of the droplet contact line during dissolution could move the droplet towards or away from the camera and thus out of focus. This led to a sudden (but as can be seen, limited) changes in the perceived droplet dimensions during the experiment which could not reliably be compensated for. However, the initial dimensions (used for further analysis) were always measured with high accuracy.

2.3. *Confocal microscopy*

To obtain insight into local concentration differences inside the dissolving droplet, confocal microscopy was employed. Confocal microscopy is an optical imaging technique which substantially increases the image resolution and contrast. Compared with a normal optical microscope, a confocal microscope can eliminate the out-of-focus light by crucially adding a pinhole on the confocal plane of the lens which acts as a filter for light from the focal plane. Three-dimensional information can be obtained by reconstruction from a series of images, taken at various focal

https://doi.org/10.1017/jfm.2016.802 Published online by Cambridge University Press

positions. Confocal, real-time observation of the dissolution process was carried out in a three-dimensional view using a 10× dry objective (Plan Fluor 10 × /0.3 DIC, numerical aperture = 0.3, working distance = 16 mm). The confocal microscope (Nikon A1 confocal laser microscope system, Nikon Corporation, Tokyo, Japan) was operated in the bottom view mode, so transparent substrates had to be used. WillCo-Dish (WillCo-Dish, The Netherlands) glass bottom dishes were used for this purpose. These dishes have a 170 μm thick borosilicate glass bottom, onto which a circular polystyrene rim is glued. The dishes were cleaned by insonication in isopropyl alcohol, ethanol and water, dried under a stream of nitrogen, and then coated with PFODMS, using the process described earlier. The polystyrene rim excludes the application of more aggressive cleaning steps. Pentanol or heptanol was premixed with cyclohexane to create a binary mixture, and a small amount of Nile red (microscopy grade, Sigma-Aldrich, the Netherlands) was added. Nile red is a hydrophobic, solvatochromic dye, which can absorb light at various wavelengths (both in the ultraviolet and visible range) and emits light at a wavelength that depends on the solvent polarity. Detecting the emitted wavelength allows us to determine if the dye is in a polar or non-polar environment, as illustrated by figure 2(*c*).

For the confocal measurements, the dish was filled with water, a single droplet of the alcohol mixture was placed on the glass bottom. Subsequently, the dish was mounted in the microscope. The Nile red dye, labelling the binary mixture, was simultaneously excited at two wavelengths $\lambda = 488$ nm and $\lambda = 561$ nm. The dye emitted light in two separate ranges: $\lambda = 500$–550 nm and $\lambda = 663$–738 nm in the pentanol-rich and cyclohexane-rich phases, respectively, which can be displayed as two different colours to visualize local concentration differences. The recording of time series three dimensional images was started after the microscope view and focus were set, which was a few minutes after deposition of the droplet. Each vertical scan loop, starting just below the droplet and scanning upward until it reaches the droplet apex, took approximately 30 s in the resonant scan mode. This time scale is much shorter than the droplet dissolution process, so that variations of the droplet morphology and size during each scan loop were small.

3. Volumetric measurements

As explained in the introduction, the dissolution rate $\mathrm{d}V/\mathrm{d}t$ in a multicomponent droplet depends on the properties of its constituents, and the composition of the droplet interface. Therefore, we can obtain information on the composition of the droplet interface by measuring the dissolution process. To this purpose, five different mixtures were prepared, listed in table 2. The first four mixtures initially contain equal amounts by volume of a soluble component (pentanol or heptanol), and a (practically) insoluble component (decanol or cyclohexane, see table 1). The fifth mixture contained two soluble components: pentanol and heptanol, also initially mixed in a 1 : 1 ratio. Besides these mixtures, single-component droplets containing either pure pentanol or pure heptanol were measured to provide a reference. All droplets had an initial volume $V_0 \approx 100$ nl. It is important to realize that pentanol, heptanol and decanol are all alcohols, and have comparable dipole moments and structures (see table 1 and figure 2*b*), whereas cyclohexane is fully apolar and has a cyclic shape.

The resulting volumes of the droplets are plotted as function of time in figure 3(*a*). Some irregularities or wiggles in the measured volumes are visible: for example in the curves representing the pentanol/heptanol mixture. These jumps are due to depinning of the droplet during dissolution, shifting the droplet slightly out of the focal plane

https://doi.org/10.1017/jfm.2016.802 Published online by Cambridge University Press

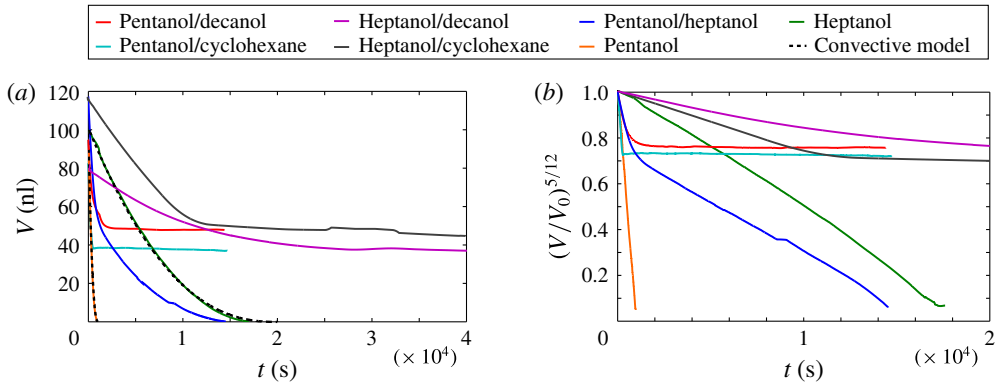


FIGURE 3. (Colour online) Volume of the droplets as function of time. All mixtures initially contain two components mixed at a 1 : 1 by volume ratio. The orange and green lines represent single-component pentanol or heptanol droplets, respectively. In panel (*b*) $(V/V_0)^{5/12}$ is plotted, resulting in straight curves for the single-component droplets, showing that they dissolve mainly through convective transport. The prefactor χ was extracted from the slope of the curves for pure pentanol and heptanol droplets, and used to plot the dashed black lines in panel (*a*), which represent the convective dissolution model, equation (3.3).

Mixture	Material a	Material b	$\frac{V_{0,a}}{V_0} : \frac{V_{0,b}}{V_0}$
1	Pentanol	Decanol	0.5 : 0.5
2	Pentanol	Cyclohexane	0.5 : 0.5
3	Heptanol	Decanol	0.5 : 0.5
4	Heptanol	Cyclohexane	0.5 : 0.5
5	Pentanol	Heptanol	0.5 : 0.5

TABLE 2. Overview of the various mixtures considered in this section. Each case represents a droplet containing materials a and b mixed with initial volumes $V_{0,a}$ and $V_{0,b}$, such that the total initial droplet volume $V_0 = V_{0,a} + V_{0,b}$.

of the microscope and changing the perceived size of the droplet. However, it should be noted that the initial dimensions of the droplet were measured with great accuracy, and that the variations due to defocussing are relatively small. In figure 3(*a*) it can be seen that the single-component droplets are completely soluble. Mixtures 1–3, which contain an insoluble component (cyclohexane or decanol), do not completely dissolve. These mixtures show an initial dissolution stage in which the soluble component dissolves and the volume of the droplets decreases. When most of the soluble material has dissolved, the dissolution rate rapidly decreases, visible as a 'kink' in the $V(t)$ curves. In the final stage, only the insoluble component remains, and the volume is constant. The heptanol/cyclohexane mixture is a surprising exception, as it appears that in this mixture also the cyclohexane slowly dissolves, for which a possible explanation will be given later. The pentanol/heptanol mixture shows a more complex behaviour, comprising a fast and a slow dissolution stage, as both of the constituents are soluble, but have one order of magnitude difference in solubility (see table 1).

https://doi.org/10.1017/jfm.2016.802 Published online by Cambridge University Press

The large difference in solubility between pentanol and heptanol results in an order of magnitude spread in the dissolution time scale, making it difficult to compare the measurements. Moreover, small differences in the initial size of the droplets affect the dissolution time. At this point it should be noted that the dissolution process described in the introduction, as well as that in the work of both Su & Needham (2013) and Chu & Prosperetti (2016) assumes a static water phase, and thus purely diffusive mass transport. In this limit, the dissolution time τ of a droplet with initial radius R_0 is approximately given by the diffusive time scale $\tau_c \equiv R_0^2 \rho_d/(2D\Delta c)$ (Zhang *et al.* 2015), where $\Delta c = c_s - c_\infty$. However, it has been shown, in the context of both growing bubbles and dissolving droplets (Enríquez *et al.* 2014; Dietrich *et al.* 2016), that a convective flow can develop, driven by solute-induced differences in the bulk density. This convective flow increases the mass exchange rate, rendering diffusive approaches inaccurate. We have shown in our recent work (Dietrich *et al.* 2016) that the effect of this convective flow on the dissolution rate is expressed by the Rayleigh number,

$$Ra \equiv \frac{g\beta_c \Delta c R^3}{\nu D}. \tag{3.1}$$

It was demonstrated that the dissolution of surface droplets is dominated by diffusive transport for low values of Ra, and dominated by convective mass transport for larger values of Ra. The cross-over between the two regimes was found to be around $Ra_t = 12$, which we call the transition Rayleigh number. In equation, (3.1) ν is the bulk viscosity, $\beta_c \equiv (\partial\rho/\partial c)/\rho_b$ is the solutal expansion coefficient of the bulk, g is the acceleration of gravity and the equivalent radius of the droplet $R = (3V/(2\pi))^{1/3}$ is chosen as its characteristic size. The initial Ra numbers of 100 nl pentanol and heptanol droplets are $Ra = 1705$ and $Ra = 170$, respectively, indicating convective dissolution.

In the convective regime, the dissolution rate of a droplet is given by (Dietrich *et al.* 2016)

$$\frac{\mathrm{d}V}{\mathrm{d}t} = -\chi (3V)^{7/12} (2\pi)^{5/12} \left(\frac{g\beta_c \Delta c_s^5 D^3}{\nu \rho_d^4} \right)^{1/4}, \tag{3.2}$$

where χ is a constant prefactor of order 1, the value of which depends on the exact shape of the droplet. Indeed it was found (Dietrich *et al.* 2016) that χ changed with the droplet contact angle. The ordinary differential equation (ODE) (3.2) can be solved to find

$$V^{5/12} = V_0^{5/12} - \frac{5\chi}{4} \left(\frac{2\pi}{3} \right)^{5/12} \left(\frac{g\beta_c \Delta c_s^5 D^3}{\nu \rho_d^4} \right)^{1/4} t. \tag{3.3}$$

If we plot $(V/V_0)^{5/12}$ as function of time for the droplets shown in figure 3(*a*), we obtain figure 3(*b*), where indeed the single-component droplets produce a straight line throughout the largest part of the dissolution process, supporting that their dissolution is described by the convective mechanism. Furthermore, we can extract the value of χ for the pure pentanol and heptanol droplets by measuring the slope of the dissolution curves in figure 3(*b*). The thus extracted values for χ are listed in table 3, and for the remainder of this work we will assume these values to be a material property, rather than a geometric one which, strictly speaking, is only correct in the limiting cases of the pure liquid droplets. The black dashed curves in figure 3(*a*) represent (3.3), evaluated using the material properties and the found values for χ for pure pentanol and heptanol droplets, showing good agreement with the experimental data.

https://doi.org/10.1017/jfm.2016.802 Published online by Cambridge University Press

Liquid	χ
Pentanol	0.65
Heptanol	0.85

TABLE 3. Values for the prefactor χ for dissolving droplets of pure pentanol and pure heptanol.

Using the thus obtained values for χ and the respective material properties one can easily calculate the convective dissolution time τ_c of a droplet with initial volume, V_0 from (3.3), giving:

$$\tau_c = \frac{4}{5\chi}\left(\frac{3V_0}{2\pi}\right)^{5/12}\left(\frac{\nu\rho_d^4}{g\beta_c\Delta c^5 D^3}\right)^{1/4}. \tag{3.4}$$

If we use the convective dissolution time to scale time in the experiments as

$$\tilde{t} = \frac{t}{\tau_c}, \tag{3.5}$$

and rescale the droplet volume by its initial volume

$$\tilde{V} = \frac{V}{V_0}, \tag{3.6}$$

and replot the data of figure 3, we obtain figure 4(*a*,*b*), where indeed the $\tilde{V}(\tilde{t})$ curves of the pure pentanol and heptanol droplets collapse, demonstrating the universality of the convective dissolution model.

For the mixtures, τ_c was calculated using the properties of material *a*, listed in table 2 and the corresponding value of χ, listed in table 3 which was assumed to be constant. Figure 4(*b*) provides a detailed view at small $\tilde{t}$, and shows that the scaled data of the single-component droplets collapse onto a single curve. Furthermore, we see that by scaling the volume according to (3.6), the residual volumes of mixtures containing either decanol or cyclohexane approximately equal $V_{0,b}/V_0$, as one expects. However, if we focus on the dissolution rate $\mathrm{d}\tilde{V}/\mathrm{d}\tilde{t}$, we see that mixtures of pentanol/decanol, heptanol/decanol and pentanol/heptanol, show a retarded dissolution as compared to the single-component droplets, owing to the addition of an insoluble or less soluble alcohol. The heptanol/cyclohexane also shows a retarded dissolution as compared to a pure heptanol droplet, however, the dissolution rate surprisingly is faster as compared to the heptanol/decanol mixture, indicating that replacing decanol by cyclohexane as the insoluble compound alters the dissolution dynamics. The retarded dissolution is not observed at all for the pentanol/cyclohexane mixture: the dissolution process of this mixture perfectly follows the $\tilde{V}(\tilde{t})$ trace of the single-component droplet. Since dissolution occurs at the droplet–bulk interface, their similar dissolution dynamics suggests that the interface of a pure pentanol droplet is identical to the pentanol/cyclohexane mixture, with pentanol fully covering the droplet's interface, i.e. comparable to a surfactant. In fact, the pentanol/cyclohexane mixture in water has been used before to study emulsions (Verhoeckx, De Bruyn & Overbeek 1987). This behaviour is consistent, for example when pentanol and cyclohexane are mixed at different initial ratios, or when the droplet is ten times larger ($V_0 = 1$ µl, instead of $V_0 = 100$ nl), as shown in figure 5.

https://doi.org/10.1017/jfm.2016.802 Published online by Cambridge University Press

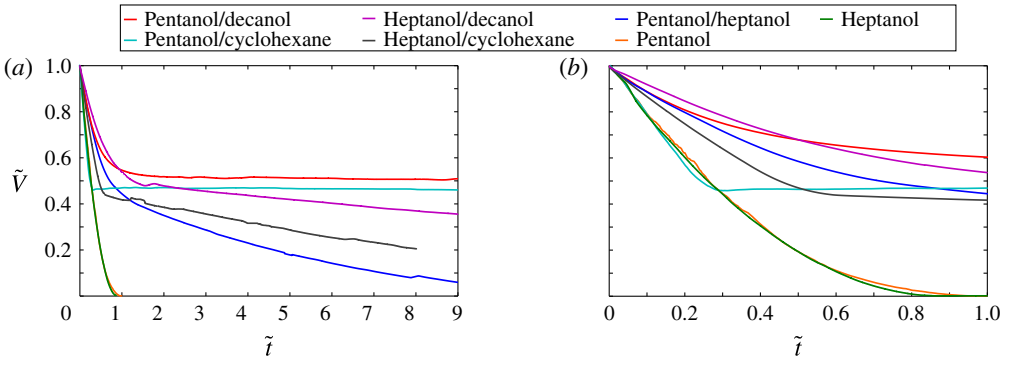


FIGURE 4. (Colour online) Scaled droplet volume $\tilde{V}(\tilde{t}) = V(t)/V_0$ as function of scaled time $\tilde{t} = t/\tau_c$ for the various mixtures, and the two single-component droplets. The single-component droplets collapse onto a single curve, illustrating universality of the convective dissolution mechanism (Dietrich *et al.* 2016). The residual volumes of each of the mixtures approximately equals $V_{0,b}/V_0$, corresponding to the fraction of insoluble material. Panel (*b*) gives a more detailed view of the interval $0 \leqslant \tilde{t} \leqslant 1$, clearly revealing that the mixtures containing two types of alcohol show retarded dissolution, whereas the mixtures containing cyclohexane do not.

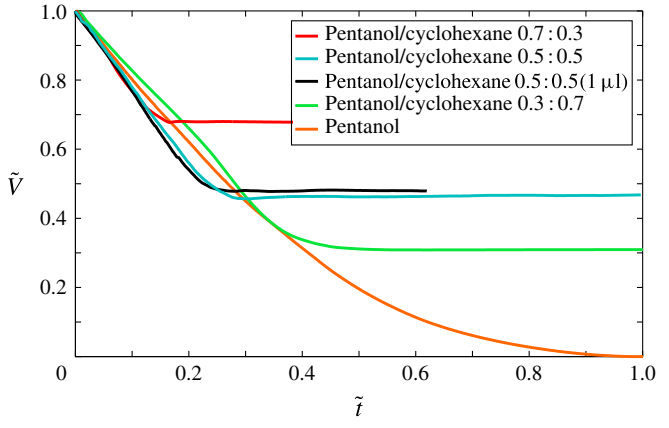


FIGURE 5. (Colour online) Scaled volume of the droplets $\tilde{V}(\tilde{t}) = V(t)/V_0$ as function of scaled time $\tilde{t} = t/\tau_c$ for pentanol/cyclohexane mixtures, and a pure pentanol droplet. Here $V_0 = 100$ nl. The mixtures are prepared at different initial compositions $V_a/V_0 : V_b/V_0$. One droplet with $V_0 = 10 \times 100$ nl $= 1$ µl was studied as well, showing identical behaviour in the rescaled variables. Each mixture, regardless its initial composition and initial volume, collapses onto the pure pentanol droplet curve during the dissolution stage, which abruptly stops at V_b/V, indicating depletion of the soluble pentanol from the droplet.

To get a more quantitative view on the segregation in the mixtures, we proceed by trying to apply the same approach as used by Su & Needham (2013), and regard the total droplet dissolution rate as the sum of the dissolution rates of the individual components. Therefore we modify (3.2) to,

$$\frac{\mathrm{d}V}{\mathrm{d}t} = \sum_{i=a,b} \frac{\mathrm{d}V_i}{\mathrm{d}t} = (2\pi)^{5/12} \sum_{i=a,b} -A_{frac,i}\chi_i (3V)^{7/12} \left(\frac{g\beta_{c,i}\Delta c_{s,i}^5 D_i^3}{\nu \rho_{d,i}^4} \right)^{1/4}, \tag{3.7}$$

https://doi.org/10.1017/jfm.2016.802 Published online by Cambridge University Press

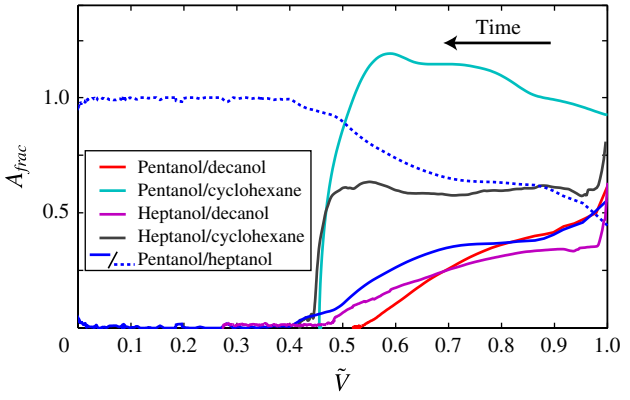


FIGURE 6. (Colour online) Interface fraction A_{frac} of the soluble component (pentanol or heptanol), as a function of scaled droplet volume $\tilde{V}$. Note that the dissolution time runs from right to left and that $A_{frac,a} > 1$ does not reflect an increase in interface area, but represents a dissolution rate larger than expected from (3.2). For the pentanol/heptanol mixture, the interface fractions of pentanol $A_{frac,pentanol}$ is plotted as the blue solid line and the interface fraction of heptanol $A_{frac,heptanol} = 1 - A_{frac,pentanol}$ is plotted as the blue dashed line. A clear distinction is observed between mixtures that contain cyclohexane on one hand, and the mixtures containing two types of alcohols on the other hand.

where the sum over $i = a, b$ indicates the summation of the contribution of the individual materials, where the material properties and values for χ as listed in tables 1 and 3 are used. $A_{frac,i} = A_i/A$ is the fraction of the interface occupied by component i at each instant in time. Since both decanol and cyclohexane are effectively insoluble, we can safely assume that in mixtures containing either of these components, all the changes in the volume of the droplet can be attributed to dissolving pentanol or heptanol. In the pentanol/heptanol mixture we use the fact that $A_{frac,heptanol} = 1 - A_{frac,pentanol}$. Equation (3.7) is fitted to the experimental data using $A_{frac,a}$ as the only fitting parameter, where again a corresponds to the materials listed in table 2. The obtained results are plotted as function of $\tilde{V}$ in figure 6. From this figure, we can distinguish two types of behaviour.

First, the mixtures that contain two types of alcohol are characterized by $A_{frac,a} = 0.5$ at $\tilde{V} = 1$, where a indicates pentanol or heptanol. This initial state is followed by a continuous decreases to $A_{frac,a} = 0$ at $\tilde{V} \approx 0.5$, signalling that (1.2) provides a good representation of the interface composition. The pentanol/heptanol mixture is somewhat more complicated to interpret, as both constituents dissolve and we cannot directly relate $\tilde{V}$ to the droplet composition. Nevertheless, as the droplet dissolves, $A_{frac,pentanol}$ (plotted as the blue solid line in figure 6) and $A_{frac,heptanol}$ (plotted as the blue dashed line in figure 6) show a continuous decrease or increase, respectively. At $\tilde{V} = 0.4$, $A_{frac,pentanol} = 0$, which is consistent with the position of the 'kink' in the dissolution curve shown in figure 4, which is followed by a decreased dissolution rate, signalling depletion of the more soluble pentanol from the droplet.

In contrast, a completely different behaviour is observed for the alcohol/cyclohexane mixtures, which display an approximately constant value for $A_{frac,a}$, followed by a steep decrease once the droplet is depleted from soluble material (at $\tilde{V} = V_b/V_0 = 0.5$). Note that $A_{frac,pentanol} > 1$, as observed for the pentanol/cyclohexane mixture, obviously does not reflect an increase in interface area, but represents a dissolution rate larger

https://doi.org/10.1017/jfm.2016.802 Published online by Cambridge University Press

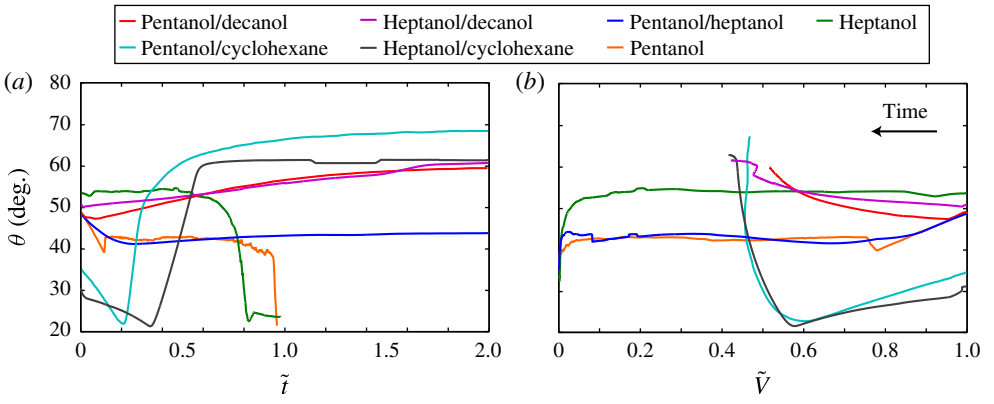


FIGURE 7. (Colour online) Contact angle θ as function of scaled time $\tilde{t}$ (*a*) and scaled droplet volume $\tilde{V}$ (*b*), during dissolution of the various mixtures. They can be compared to the values of the pure components: $43^\circ \leqslant \theta \leqslant 50^\circ$ and $50^\circ \leqslant \theta \leqslant 60^\circ$ for pentanol and heptanol, respectively.

than expected from (3.2), possibly caused by increased convection, which we will demonstrate later on. The behaviour of $A_{frac,heptanol}$ in the heptanol/cyclohexane mixture is consistent with the dissolution dynamics observed in figure 4, where the dissolution of the heptanol/cyclohexane mixture was slower than the pure heptanol droplet, but did show a sharp kink, marking the point at which heptanol was depleted from the droplet. This heptanol/cyclohexane mixture displays some more surprising features. Figure 4 shows that for $\tilde{V} < 0.5$ the cyclohexane does in fact dissolve. A intriguing similar behaviour was observed in preliminary measurements on pentanol/cyclohexane droplets in water presaturated to $0.5 \times c_s$ pentanol. We hypothesize that heptanol, and to a lesser extent pentanol, acts as a surfactant that helps to disperse cyclohexane in water. A large affinity between heptanol and cyclohexane could also explain the reduced dissolution rate of this mixture observed in figure 4. However, more work is required to verify this.

Chu & Prosperetti (2016) numerically evaluated the surface composition of their dissolving binary droplets. They demonstrated that the concentration of species at the droplet surface was often not equal to the concentration inside the droplet, and was related to the activity coefficient, which expresses the affinity between the droplet constituents and the bulk. Even though Chu and Prosperetti considered other droplet materials than those used in the current work, it is striking to see that their theoretical predictions for the composition are qualitatively similar to the $A_{frac}(\tilde{V})$ curves extracted from our experiments. Clearly, future work should involve a direct comparison between theory and experiment, by performing evaporation or dissolution experiments on the identical combinations of droplet materials as those in the work by Chu and Prosperetti.

4. Segregation, contact angle and Marangoni flow

Given the difference in surface tensions for the liquids, the change in interface composition should result in a change of the contact angle θ. This change is easily confirmed by plotting θ as function of $\tilde{t}$, as done in figure 7. Figure 7 again shows distinctive behaviour between droplets containing mixtures of alcohols and

https://doi.org/10.1017/jfm.2016.802 Published online by Cambridge University Press

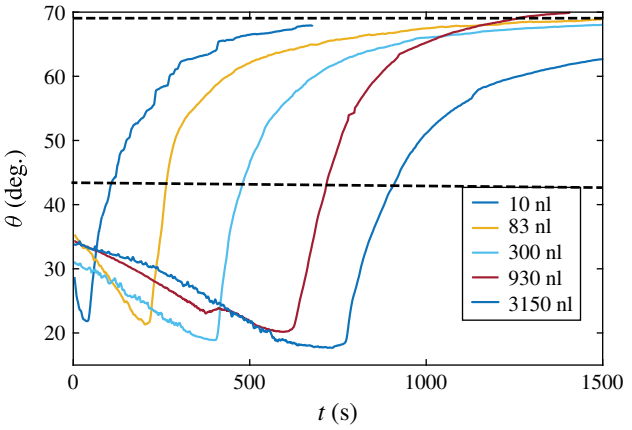


FIGURE 8. (Colour online) Contact angle θ as function of time $\tilde{t}$, during dissolution of mixture two droplets, initially containing a mixture of equal amounts of pentanol and cyclohexane. The dashed lines indicate the receding contact angles θ_R for pure droplets of pentanol ($\theta_R = 43°$) and cyclohexane ($\theta_R = 69°$).

the droplets containing cyclohexane: contact angles for mixtures of pentanol/decanol, heptanol/decanol and pentanol/heptanol are always limited by the values of the pure components (listed in table 1). The pentanol/cyclohexane mixture shows a sharp decrease towards $\theta < 30°$, far below the value for either pure pentanol or cyclohexane. This decrease in θ could be the result of initial spreading of the droplet, during which the footprint radius increases and θ slowly decreases to an equilibrium value. However, if we look at figure 1(*d*), we see that an increase in the footprint radius is not observed, and therefore cannot explain the decrease in θ. Moreover, the values of the receding contact angles θ_R, as listed in table 1, are all $> 30°$, excluding contact line pinning as an explanation for the low contact angle. Also the (initial) volume of the droplet does not affect the contact angles, as demonstrated by figure 8, where θ is plotted as function of time for pentanol/cyclohexane droplets with varying initial volumes.

As the decrease in θ is not observed in immersed sessile droplets of either pure pentanol or cyclohexane, it is possible that this remarkable behaviour of θ for the cyclohexane–alcohol droplets is related to segregation of the two components. Segregation between the components can be visualized by adding a small amount of solvatochromic dye to the pentanol/cyclohexane mixture, and visualize the droplet during dissolution using confocal microscopy. From this, we obtain a three-dimensional profile of the droplet surface, where the colour of the dye represents the composition, as shown in figure 9. In this figure, the purple colour (representing pentanol-rich regions) initially covers the entire surface, as shown in figure 9(*a*). During dissolution (figure 9*b*), the perimeter of the droplet turns yellow, representing an increase of the cyclohexane concentration in this region. The depletion of soluble material and the enrichment of cyclohexane near the contact line indicates that, similar to diffusive dissolution (Popov 2005; Hu & Larson 2002; Gelderblom *et al.* 2011), convective dissolution in this case leads to an increased flux of the soluble material at the droplet perimeter. As dissolution progresses and more pentanol dissolves, the cyclohexane rim rapidly expands inward (figure 9*b*,*c*), until ultimately all pentanol has dissolved (figure 9*d*). Depletion of the soluble component from the droplet

https://doi.org/10.1017/jfm.2016.802 Published online by Cambridge University Press

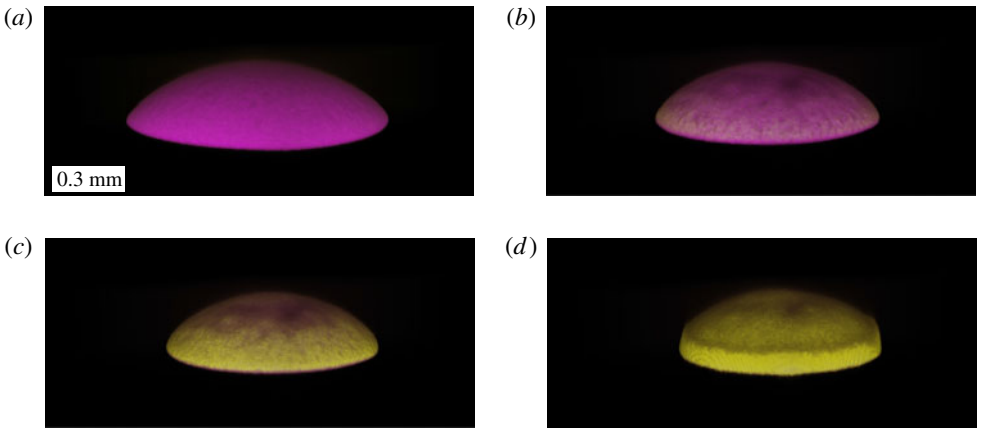


FIGURE 9. (Colour online) Three-dimensional confocal image of a droplet containing a pentanol/cyclohexane mixture. Panels show the surface at $t = 0$ s (*a*), $t = 270$ s (*b*), $t = 360$ s (*c*) and $t = 420$ s (*d*). Purple indicates the polar solvent (pentanol), yellow indicates the non-polar solvent (cyclohexane). The surface is covered with pentanol during a large fraction of the dissolution process, with depletion starting from the rim (*b* and *c*).

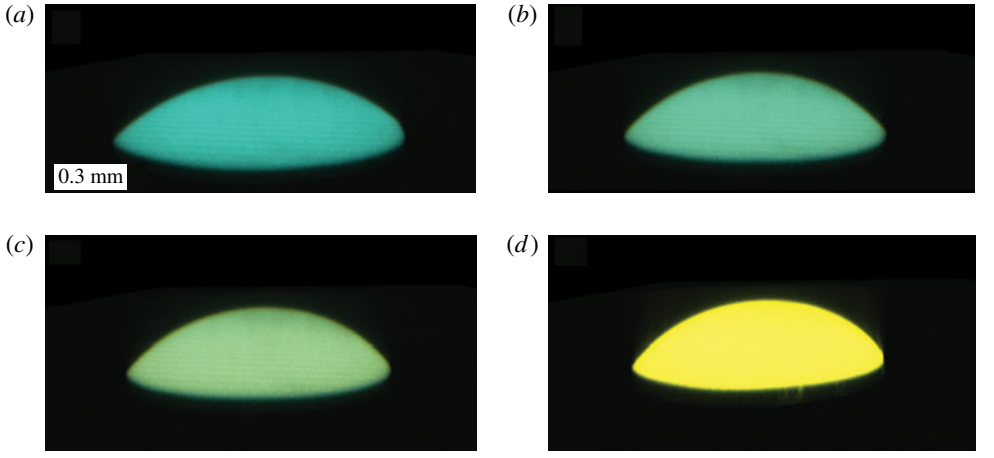


FIGURE 10. (Colour online) Three-dimensional representation of the droplet surface at $t = 0$ s (*a*), $t = 2000$ s (*b*), $t = 3300$ s (*c*) and $t = 6000$ s (*d*). Blue indicates heptanol, yellow indicates cyclohexane. The uniform green appearance in panels (*b*) and (*c*) indicates a well-mixed interface during dissolution.

interface is not readily observed when we perform the same measurement for a droplet of heptanol/cyclohexane mixture, shown in figure 10. The surface of this droplet shows a continuous, uniform transition from blue/green (representing a high heptanol concentration), to yellow.

The difference in concentration over the droplet interface, combined with the large difference in surface tension of the two liquids, leads to an interfacial tension gradient over the interface. This gradient results in a Marangoni flow across the interface, directed from the droplet apex towards the rim. It is this flow that results in the so-called superspreading of the droplet (Nikolov *et al.* 2002; Hernández-Sánchez,

https://doi.org/10.1017/jfm.2016.802 Published online by Cambridge University Press

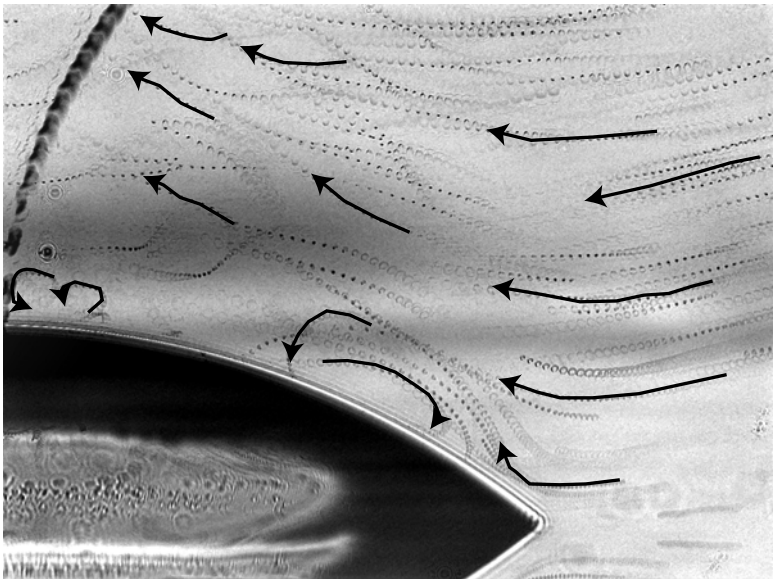


FIGURE 11. Streak image, showing the motion of tracer particles added to the bulk, surrounding a dissolving droplet containing a mixture of pentanol and cyclohexane. Arrows are drawn to indicate the direction of the particle trajectories. Most of the particles flow right to left, accumulating in a single convective plume rising upward from the droplet apex. Some particles, close to the droplet–bulk interface, recirculate due to the Marangoni flow across the droplet interface.

Eddi & Snoeijer 2015; Tsoumpas *et al.* 2015). We can confirm the presence of this interfacial flow by two experiments. Firstly, the bulk flow can be visualized by adding a small amount of tracer particles (3 μm diameter, fluoromax Thermoscientific) to the water. Figure 11 shows a streak image which readily demonstrates that while the bulk flows towards the droplet apex (consistent with convective droplet dissolution (Dietrich *et al.* 2016)), particles close to the droplet interface swirl around and move in the opposite direction, as indicated by the arrows. (Unfortunately, the low particle concentration near the droplet interface prohibited detailed particle image velocimetry or particle tracking.) Secondly, by slightly defocussing the microscope, a shadowgraph image is recorded, which shows local differences in optical index (caused by dissolved alcohol) as brighter/darker regions. Such a shadowgraph is shown in figure 12: the large plume above the droplet is the alcohol-rich convective plume, which moves upward driven by a solute-induced buoyant force. This convection draws in fresh water from the sides. The smaller flame-like features visible just above the interface are small swirls, which propagate in the opposite direction from the bulk, as indicated by the arrows. These swirls create an extra convection in the solute-rich boundary layer that develops over the dissolving droplet. In the absence of these swirls, the boundary layer is laminar, and mass transport is driven by diffusion, perpendicular to the droplet interface. The swirls thus enhance the mass transport through the boundary layer. As the convective dissolution model is based on the assumption of a laminar boundary layer, it is to be expected that the presence of convection increases mass transport to values above those expected based on (3.3), and from that the fitted value $A_{frac,pentanol} > 1$ for the pentanol/cyclohexane mixture.

https://doi.org/10.1017/jfm.2016.802 Published online by Cambridge University Press

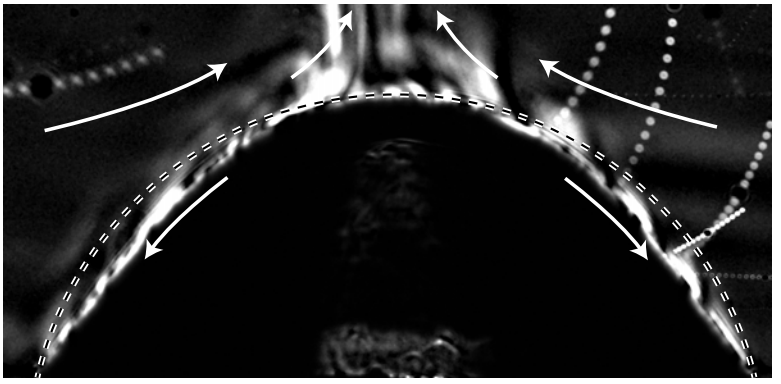


FIGURE 12. Shadowgraphy image (filtered and contrast enhanced) of a dissolving droplet containing a mixture of pentanol and decanol. Deformation of the droplet, caused by Marangoni flow and local differences in surface tension, is visible as the non-spherical cap shape (drawn as the dashed line in the figure) of the droplet.

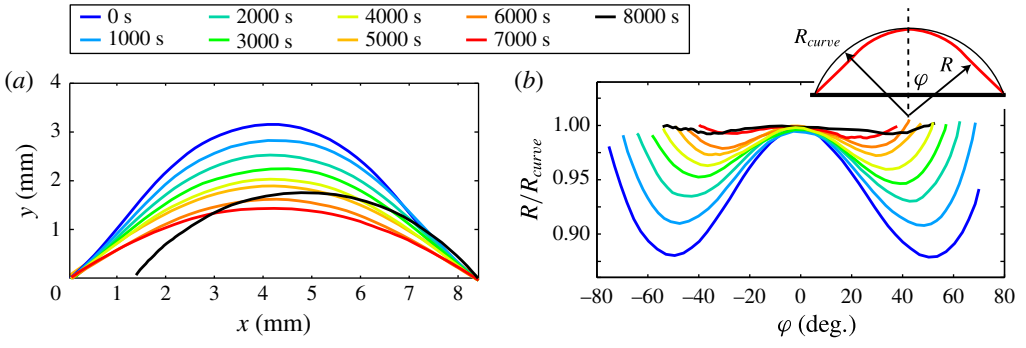


FIGURE 13. (Colour online) (*a*) Profiles of a droplet containing a pentanol/cyclohexane mixture at subsequent times. At early times, the droplet shape deviates from spherical cap shape. This is quantified in panel (*b*), where the droplet radius $R(\phi)$ is compared to the radius of curvature R_{curve} of a spherical cap (as sketched in the inset, where red indicates the droplet shape and black the spherical cap). Only at the end of the experiment, when the pentanol has dissolved, the droplet takes the spherical cap shape, as indicated by the black curve in panel (*b*), with $R/R_{curve} \approx 1$.

Figure 13 illustrates another effect in a droplet (containing pentanol and cyclohexane) caused by the depleted rim, which only becomes clear for large droplets ($V \geqslant 5$ µl): locally varying surface tensions and the Marangoni flow cause the droplet shape to deviate from a spherical cap, with an increased radius of curvature near the contact line (Nikolov *et al.* 2002). Figure 13(*a*) shows the droplet profiles at subsequent times, and illustrates how the Marangoni flow causes a wide footprint radius (which is pinned during the dissolution), and contact angles with values below θ_R. At the end of the dissolution, when no concentration differences exits, the Marangoni flow stops, the contact line depins and the droplet assumes a spherical cap shape (black curve, $t = 8000$ s). From the profiles at early times (blue profile) one sees that the radius of curvature at the droplet apex is markedly different than

https://doi.org/10.1017/jfm.2016.802 Published online by Cambridge University Press

the curvature near the contact line. This difference is quantified in figure 13(*b*): the radius R of the droplet (sketched in red in the inset in *b*) is measured as function of ϕ, the angle with respect to the surface normal. R is compared to the radius of curvature R_{curve} of a spherical cap with identical footprint diameter and height as the droplet under consideration (sketched in black in the inset). For a spherical cap shaped droplet, this analysis would lead to a straight line at $R/R_{curve} = 1$, which is only observed at the end of the experiment (black curve in panel (*b*), at 8000 s), when all soluble pentanol has dissolved and a droplet of pure cyclohexane remains. At earlier times, the radius shows dimples near the contact line, indicating a deviation from a spherical cap, and deformation of the droplet near the contact line.

5. Discussion and conclusion

In the current work we have shown that dissolving droplets containing different binary mixtures of liquids can exhibit markedly different behaviour depending on the droplet's constituents. We have shown that the approach of Su & Needham (2013) is justified for some, but not for all, mixtures: in the case of mixtures containing two comparable liquids, such as two different types of alcohols, the interfacial composition of the droplet indeed depends on, and varies continuously with, the droplet composition. However, this does not hold for all mixtures, like the alcohol/cyclohexane mixtures considered in this work. It thus appears that the assumption, reflected in (1.2) is only valid for mixtures of components with comparable material parameters, such as polarity and surface tension with the bulk. More work is required to explore to which limits (1.2) is valid, and a description of the dissolution process such as (3.7) is applicable.

Clearly, the alcohol/cyclohexane mixtures in this work showed segregation of the droplet constituents: in these cases, a constant surface composition was measured during dissolution, regardless of the droplet composition, and in these situations the method proposed by Chu & Prosperetti (2016) is likely to be more accurate. The next step would therefore consist of experiments on binary mixtures and matching these to simulations to allow for a direct comparison. However, we have also shown that more complicated processes should be considered, as strong dynamical effects can occur. Our confocal microscopy measurements have revealed that local depletion of the soluble compound occurs, which in turn fuels a Marangoni flow. Especially this last observation can have huge implications, either undesirable or advantageous, for example for ink droplets containing pigments which should be distributed evenly over the substrate. Lastly, our measurements hint at the possibility that the soluble component can act as a surfactant to the non-soluble component, likely compromising the accuracy of current theories. These effects illustrate the finding that in many applications – some of which such as liquid–liquid microextraction were discussed in Lohse (2016) – the interaction between the droplet constituents and the bulk cannot be neglected.

Acknowledgements

X. Zhang and A. Prosperetti are acknowledged for many stimulating discussions. Funding from The Netherlands Organisation for Scientific Research (NWO, project no. 11431) and the zwaartekracht MCEC program is acknowledged.

https://doi.org/10.1017/jfm.2016.802 Published online by Cambridge University Press

REFERENCES

ABRAMZON, B. & SIRIGNANO, W. A. 1989 Droplet vaporization model for spray combustion calculations. *Intl J. Heat Mass Transfer* **32**, 1605–1618.

ADDISON, C. C. & HUTCHINSON, S. K. 1949 The properties of freshly formed surfaces. part xi. factors influencing surface activity and adsorption rates in aqueous decyl alcohol solutions. *J. Chem. Soc.* 3387–3395.

AGGARWAL, S. K. & PENG, F. 1995 A review of droplet dynamics and vaporization modeling for engineering calculations. *J. Engng Gas Turbines Power* **117**, 453–461.

VAN DER BOS, A., VAN DER MEULEN, M.-J., DRIESSEN, T., VAN DEN BERG, M., REINTEN, H., WIJSHOFF, H., VERSLUIS, M. & LOHSE, D. 2014 Velocity profile inside piezoacoustic inkjet droplets in flight: comparison between experiment and numerical simulation. *Phys. Rev. Appl.* **1**, 014004.

BOURGES-MONNIER, C. & SHANAHAN, M. E. R. 1995 Influence of evaporation on contact angle. *Langmuir* **11** (7), 2820–2829.

BRENN, G., DEVIPRASATH, L. J., DURST, F. & FINK, C. 2007 Evaporation of acoustically levitated multi-component liquid droplets. *Intl J. Heat Mass Transfer* **50**, 5073–5086.

BURGER, M., SCHMEHL, R., PROMMERSBERGER, K., SCHÄFER, O., KOCH, R. & WITTIG, S. 2003 Droplet evaporation modeling by the distillation curve model: accounting for kerosene fuel and elevated pressures. *Intl J. Heat Mass Transfer* **46**, 4403–4412.

CAZABAT, A.-M. & GUENA, G. 2010 Evaporation of macroscopic sessile droplets. *Soft Matt.* **6**, 2591–2612.

CHU, S. & PROSPERETTI, A. 2016 Dissolution and growth of a multicomponent drop in an immiscible liquid. *J. Fluid Mech.* **798**, 787–811.

CRITTENDEN, E. D. JR. & HIXSON, A. N. 1954 Extraction of hydrogen chloride from aqueous solutions. *Ind. Engng Chem.* **46**, 265–274.

DEHAECK, S., REDNIKOV, A. & COLINET, P. 2014 Vapor-based interferometric measurement of local evaporation rate and interfacial temperature of evaporating droplets. *Langmuir* **30**, 2002–2008.

DEMOND, A. H. & LINDNER, A. S. 1993 Estimation of interfacial tension between organic liquids and water. *Environ. Sci. Technol.* **27** (12), 2318–2331.

DIETRICH, E., KOOIJ, E. S., ZHANG, X., ZANDVLIET, H. J. W. & LOHSE, D. 2015 Stick-jump mode in surface droplet dissolution. *Langmuir* **31** (16), 4696–4703.

DIETRICH, E., WILDEMAN, S., VISSER, C. W., HOFHUIS, K., KOOIJ, E. S., ZANDVLIET, H. J. W. & LOHSE, D. 2016 Role of natural convection in the dissolution of sessile droplets. *J. Fluid Mech.* **794**, 45–67.

DUNN, G. J., WILSON, S. K., DUFFY, B. R., DAVID, S. & SEFIANE, K. 2009 The strong influence of substrate conductivity on droplet evaporation. *J. Fluid Mech.* **623**, 329–351.

ENRÍQUEZ, O. R., SUN, C., LOHSE, D., PROSPERETTI, A. & VAN DER MEER, D. 2014 The quasi-static growth of CO_2 bubbles. *J. Fluid Mech.* **741**.

EPSTEIN, P. S. & PLESSET, M. S. 1950 On the stability of gas bubbles in liquid–gas solutions. *J. Chem. Phys.* **18**, 1505–1509.

ERBIL, H. Y. 2012 Evaporation of pure liquid sessile and spherical suspended drops: a review. *Adv. Colloid Interface Sci.* **170**, 67–86.

GELDERBLOM, H., MARÍN, Á. G., NAIR, H., VAN HOUSELT, A., LEFFERTS, L., SNOEIJER, J. H. & LOHSE, D. 2011 How water droplets evaporate on a superhydrophobic substrate. *Phys. Rev.* E **83**, 026306.

GSI ENVIRONMENTAL 2016 Gsi environmental chemical database. www.gsi-net.com/en/publications/gsi-chemical-database/single/152.html.

GUÉNA, G., POULARD, C. & CAZABAT, A.-M. 2006 The leading edge of evaporating droplets. *J. Colloid Interface Sci.* **312**, 164–171.

HANSCH, C., QUINLAN, J. E. & LAWRENCE, G. L. 1968 Linear free-energy relationship between partition coefficients and the aqueous solubility of organic liquids. *J. Org. Chem.* **33** (1), 347–350.

HAO, L. & LEAIST, D. G. 1996 Binary mutual diffusion coefficients of aqueous alcohols. Methanol to 1-heptanol. *J. Chem. Engng Data* **41** (2), 210–213.

https://doi.org/10.1017/jfm.2016.802 Published online by Cambridge University Press

HASTINGS, J., DE MATOS, P., DEKKER, A., ENNIS, M., HARSHA, B., KALE, N., MUTHUKRISHNAN, V., OWEN, G., TURNER, S., WILLIAMS, M. *et al.* 2013 The chebi reference database and ontology for biologically relevant chemistry: enhancements for 2013. *Nucleic Acids Res.*

HAYNES, W. M. 2004 *Handbook of Chemistry and Physics*. CRC.

HERNÁNDEZ-SÁNCHEZ, J. F., EDDI, A. & SNOEIJER, J. H. 2015 Marangoni spreading due to a localized alcohol supply on a thin water film. *Phys. Fluids* **27**, 032003.

HØILAND, H. & VIKINGSTAD, E. 1976 Partial molal volumes and additivity of group partial molal volumes of alcohols in aqueous solution at 25 °C and 35 °C. *Acta Chem. Scand.* A **30**, 182–186.

HU, H. & LARSON, R. G. 2002 Evaporation of a sessile droplet on a substrate. *J. Phys. Chem.* B **106** (6), 1334–1344.

KELLY-ZION, P., BATRA, J. & PURSELL, C. J. 2013 Correlation for the convective and diffusive evaporation of a sessile drop. *Engineering Faculty Research* **5**, 278–285.

KELLY-ZION, P. L., PURSELL, C. J., BOOTH, R. S. & VANTILBURG, A. N. 2009 Evaporation rates of pure hydrocarbon liquids under the influences of natural convection and diffusion. *Intl J. Heat Mass Transfer* **52** (13–14), 3305–3313.

KINOSHITA, K., ISHIKAWA, H. & SHINODA, K. 1958 Solubility of alcohols in water determined by the surface tension measurements. *Bull. Chem. Soc. Jpn.* **31** (9), 1081–1082.

KNEER, R., SCHNEIDER, M., NOLL, B. & WITTIG, S. 1993 Diffusion controlled evaporation of a multicomponent droplet: theoretical studies on the importance of variable liquid properties. *Intl J. Heat Mass Transfer* **36** (9), 2403–2415.

LEHMANN, S., LORENZ, S., RIVARD, E. & BRÜGGEMANN, D. 2015 Experimental analysis and semicontinuous simulation of low temperature droplet evaporation of multicomponent fuels. *Exp. Fluids* **56**, 1871.

LOHSE, D. 2016 Towards controlled liquid–liquid microextraction. *J. Fluid Mech.* **804**, 1–4.

LOHSE, D. & ZHANG, X. 2015 Surface nanobubbles and nanodroplets. *Rev. Mod. Phys.* **87**, 981–1035.

MOFFAT, J. R., SEFIANE, K. & SHANAHAN, M. E. R. 2009 Effect of TiO_2 nanoparticles on contact line stick-slip behavior of volatile drops. *J. Phys. Chem.* B **113** (26), 8860–8866.

NGUYEN, T. A. H. & NGUYEN, A. V. 2012 Increased evaporation kinetics of sessile droplets by using nanoparticles. *Langmuir* **28** (49), 16725–16728.

NIKOLOV, A. D., WASAN, D. T., CHENGARA, A., KOCZO, K., POLICELLO, G. A. & KOLOSSVARY, I. 2002 Superspreading driven by Marangoni flow. *Adv. Colloid Interface Sci.* **96** (1), 325–338.

PICKNETT, R. G. & BEXON, R. 1977 The evaporation of sessile or pendant drops in still air. *J. Colloid Interface Sci.* **61** (2), 336–350.

POPOV, Y. O. 2005 Evaporative deposition patterns: spatial dimensions of the deposit. *Phys. Rev.* E **71**, 036313.

SAZHIN, S. S., ELWARDANY, A., PRUTITSKII, P. A., CASTANET, G., LEMOINE, F., SAZHINA, E. M. & HEIKAL, M. R. 2010 A simplified model for bi-component droplet heating and evaporation. *Intl J. Heat Mass Transfer* **53**, 4495–4505.

SHANAHAN, M. E. R. 1995 Simple theory of 'stick-slip' wetting hysteresis. *Langmuir* **11** (3), 1041–1043.

SOBAC, B. & BRUTIN, D. 2012 Thermal effects of the substrate on water droplet evaporation. *Phys. Rev.* E **86**, 021602.

SOMASUNDARAM, S., ANAND, T. N. C. & BAKSHI, S. 2015 Evaporation-induced flow around a pendant droplet and its influence on evaporation. *Phys. Fluids* **27**, 112105.

STAUBER, J. M., WILSON, S. K., DUFFY, B. R. & SEFIANE, K. 2014 On the lifetimes of evaporating droplets. *J. Fluid Mech.* **744**, R2.

STAUBER, J. M., WILSON, S. K. & DUFFY, B. R. 2015*a* Evaporation of droplets on strongly hydrophobic substrates. *Langmuir* **31** (12), 3653–3660.

STAUBER, J. M., WILSON, S. K., DUFFY, B. R. & SEFIANE, K. 2015*b* On the lifetimes of evaporating droplets with related initial and receding contact angles. *Phys. Fluids* **27**, 122101.

STENUTZ, R. 2015 Structure and physical data for decanol. *Tables for Chemical Species*. http://www.stenutz.eu/chem/solv6.php?name=decanol.

https://doi.org/10.1017/jfm.2016.802 Published online by Cambridge University Press

SU, J. T. & NEEDHAM, D. 2013 Mass transfer in the dissolution of a multicomponent liquid droplet in an immiscible liquid environment. *Langmuir* **29** (44), 13339–13345.

TALBOT, E. L., BERSON, A., BROWN, P. S. & BAIN, C. D. 2012 Evaporation of picoliter droplets on surfaces with a range of wettabilities and thermal conductivities. *Phys. Rev.* E **85**, 061604.

TAMIM, J. & HALLETT, W. L. H. 1995 A continuous thermodynamic model for multicomponent droplet vaporization. *Chem. Engng Sci.* **50**, 2933–2942.

TAN, H., DIDDENS, C., LV, P., KUERTEN, J. G. M., ZHANG, X. & LOHSE, D. 2016 Evaporation-triggered microdroplet nucleation and the four life phases of an evaporating ouzo drop. *Proc. Natl Acad. Sci. USA* **113**, 8642–8647.

TONINI, S. & COSSALI, G. E. 2015 A novel formulation of multi-component drop evaporation models for spray applications. *Intl J. Therm. Sci.* **89**, 245–253.

TONINI, S. & COSSALI, G. C. 2016 A multi-component drop evaporation model based on analytical solution of stefan-maxwell equations. *Intl J. Heat Mass Transfer* **92**, 184–189.

TSOUMPAS, Y., DEHAECK, S., REDNIKOV, A. & COLINET, P. 2015 Effect of marangoni flows on the shape of thin sessile droplets evaporating into air. *Langmuir* **31** (49), 13334–13340.

VERHOECKX, G. J., DE BRUYN, P. L. & OVERBEEK, J. TH. G. 1987 On understanding microemulsions. *J. Colloid Interface Sci.* **119**, 409–421.

YAWS, C. L. 2014 *Thermophysical Properties of Chemicals and Hydrocarbons*. Elsevier/Gulf Professional Publishing.

ZHANG, L. & KONG, S.-C. 2012 Multicomponent vaporization modeling of bio-oil and its mixtures with other fuels. *Fuel* **95**, 471–480.

ZHANG, X., WANG, J., BAO, L., DIETRICH, E., VAN DER VEEN, R. C. A., PENG, S., FRIEND, J., ZANDVLIET, H. J. W., YEO, L. & LOHSE, D. 2015 Mixed mode of dissolving immersed nanodroplets at a solid-water interface. *Soft Matt.* **11**, 1889–1900.

https://doi.org/10.1017/jfm.2016.802 Published online by Cambridge University Press